Published in final edited form as:
J Biol Inorg Chem. 2012 April ; 17(4): 647–662. doi:10.1007/s00775-012-0885-0.

Laue Crystal Structure of *Shewanella oneidensis* Cytochrome *c* Nitrite Reductase from a High-yield Expression System

Matthew Youngblut[1], **Evan T. Judd**[3], **Vukica Srajer**[4], **Bilal Sayyed**[1], **Tyler Goelzer**[1], **Sean J. Elliott**[3,*], **Marius Schmidt**[2,*], and **A. Andrew Pacheco**[1,*]

[1]Department of Chemistry and Biochemistry, 3210 N. Cramer St, University of Wisconsin-Milwaukee, Milwaukee, WI 53211

[2]Department of Physics, 1900 E. Kenwood Blvd, University of Wisconsin-Milwaukee, Milwaukee, WI 53211

[3]Department of Chemistry, 590 Commonwealth Ave., Boston, MA 02215

[4]Center for Advanced Radiation Sources, The University of Chicago, Chicago, IL 60637, USA

Abstract

The high-yield expression and purification of *Shewanella oneidensis* cytochrome *c* nitrite reductase (ccNiR), and its characterization by a variety of methods, notably Laue crystallography, is reported. A key component of the expression system is an artificial ccNiR gene in which the N-terminal signal peptide from the highly expressed *S. oneidensis* protein "Small Tetra-heme *c*" replaces the wild-type signal peptide. This gene, inserted into the plasmid pHSG298 and expressed in *S. oneidensis* TSP-1 strain, generated ~20 mg crude ccNiR/L culture, compared with 0.5–1 mg/L for untransformed cells. Purified ccNiR has nitrite and hydroxylamine reductase activities comparable to those previously reported for *E. coli* ccNiR, and is stable for over two weeks in pH 7 solution at 4° C. UV/Vis spectropotentiometric titrations and protein film voltammetry identified 5 independent 1-electron reduction processes. Global analysis of the spectropotentiometric data also allowed determination of the extinction coefficient spectra for the 5 reduced ccNiR species. The characteristics of the individual extinction coefficient spectra suggest that, within each reduced species, the electrons are distributed amongst the various hemes, rather than being localized on specific heme centers. The purified ccNiR yielded good quality crystals, with which the 2.59 Å resolution structure was solved at room temperature using the Laue diffraction method. The structure is similar to that of *E. coli* ccNiR, except in the region where the enzyme interacts with its physiological electron donor (CymA in the case of *S. oneidensis* ccNiR, NrfB in the case of the *E. coli* protein).

Keywords

Cytochrome *c* nitrite reductase; NrfA; Laue crystallography; UV/Vis spectropotentiometry; Protein film voltammetry

Introduction

Ammonia-nitrite interconversion, an important part of the biological nitrogen cycle, is carried out by a variety of bacteria as part of their respiratory process. In one direction the

AAP apacheco@uwm.edu; Ph: 414-229-4413; Fax: 414-229-5530. MS m-schmidt@uwm.edu; Ph: 414-229-4338; Fax: 414-229-5589. SJE elliott@bu.edu; Ph: 617-358-2816; Fax: 617-353-6466.

ammonia oxidizing bacteria (AOB) such as *Nitrosomonas europaea* use ammonia as an electron donor in respiration, and oxidize it to nitrite [1]. A different class of bacteria uses nitrite as a terminal electron acceptor in the absence of oxygen, reducing it to ammonia in a process known as nitrite ammonification [2]. Hydroxylamine oxidoreductase (HAO), the AOB enzyme that catalyzes the 4-electron oxidation of hydroxylamine to nitrite, shows some structural similarities to the enzyme cytochrome *c* nitrite reductase (ccNiR, also called NrfA), which catalyzes the 6-electron reduction of nitrite to ammonia in ammonifying bacteria [3–10]. Moreover, formal catalytic cycles suggest that HAO and ccNiR probably go through many comparable reactive intermediates [11, 12]. Given the structural similarities between HAO and ccNiR, and the fact that they catalyze similar reactions in opposing directions, our research group is undertaking a long-term comparative study of HAO and ccNiR, aimed at determining how each enzyme is optimized to preferentially operate in one or the other direction. In two recent papers we described experiments in which HAO was forced to run in reverse (as a ccNiR) [12, 13]; herein we turn our attention towards ccNiR, and lay the groundwork for using the powerful evolving technique of Laue crystallography to study this enzyme in action.

CcNiR catalyzes the six-electron reduction of nitrite to ammonia (Scheme 1, Eq. 1), as well as the five-electron reduction of nitric oxide (Scheme 1, Eq. 2) and the two-electron reduction of hydroxylamine (Scheme 1, Eq. 3) to ammonia [11, 14]. The enzyme has also been shown to perform the six-electron reduction of sulfite to sulfide (Scheme 1, Eq. 4), albeit at much lower rates [15]. CcNiR is a soluble homodimeric protein that contains 5 hemes per monomer (Fig. 1). The molecular weight of a ccNiR monomer ranges from 52–65 kDa, depending on the bacterial species from which it was isolated. A number of crystal structures of the enzyme are available [3–9], that share many features in common. The ccNiR active site is a 5-coordinate heme with the unusual axial ligand lysine in the proximal position. During catalysis the substrate binds to the distal position and is reduced. The remaining four hemes in each subunit are all typical 6-coordinate *c*-type hemes with two His ligands each. These hemes are low-spin and closely spaced, so they can efficiently shuttle electrons to the active site. An interesting feature of the hemes used solely for electron transport is that in all known ccNiR structures they form two branches leading to the active site. Furthermore, this branched pattern is seen not just in the ccNiRs, but also in HAO [10]. From our HAO studies we have proposed that the branching hemes allow electrons to be added or removed from the active site in pairs, with each electron in a pair traveling along a different branch, in order to minimize Coulomb repulsion between the electrons (Fig. 1) [16].

A reaction mechanism for the catalytic reduction of nitrite by ccNiR was proposed in 2002 based on crystallographic and computational analysis [11], and this mechanism has recently been refined on the basis of a detailed density-functional study of the first reduction step [17]. The mechanistic scheme is buttressed by extensive literature precedent in other biological and heme model systems [18, 19], and serves as an excellent starting point for guiding future research. Moreover, a formally comparable catalytic cycle can be used as the starting point for guiding the investigation of HAO-catalyzed hydroxylamine oxidation [12, 13].

Laue crystallography is potentially a very powerful tool for investigating redox-active enzymes such as ccNiR. During data collection in conventional crystallography, the crystal is exposed to monochromatic X-rays for an extended period of time, in the range of several tens of minutes to hours for a bright source such as that available at a synchrotron. However, exposing a crystal to X-rays often changes the crystal on the time scale of the conventional experiment; in particular, metalloproteins such as ccNiR and HAO are extremely susceptible to photoreduction in an X-ray beam [20–22]. As a result, the structure one obtains from

crystallography is often not that of the original molecule. Instead it reflects the average of the original structure and those of the protein after modification by the X-rays. In photography an analogy would be the photograph of a moving object taken at a slow shutter speed: such a photograph would be blurred because it would show the object in several positions at once. By contrast, using the Laue method is analogous to taking the same photograph with a fast shutter speed. A Laue diffraction pattern is obtained by exposing a crystal to polychromatic X-rays for only 100 ps, too short a time for radiation damage to appear. As a consequence, the Laue method is ideally suited to the investigation of proteins such as ccNiR and HAO that are susceptible to X-ray damage. Another major advantage of the Laue method is that it can be used to monitor reactions within crystals as a function of time [23–36], which is possible because Laue diffraction patterns are collected over very short time scales. If a reaction can be rapidly initiated within a crystal, for example by using a laser to activate a photochemical trigger, then a Laue diffraction pattern can provide the crystal structure at a defined time after reaction initiation. By piecing together Laue patterns obtained at different times after initiation, a time-resolved sequence can be obtained. One other feature aids in the logistics of applying the Laue technique. Since the polychromatic X-ray beam used in Laue crystallography is tightly focused, it typically strikes only a small part of the crystal in a given experiment. Consequently, the same crystal can be used for several experiments, simply by moving the crystal so that the beam strikes a different region each time.

One long-term goal in our investigation of ammonia-nitrite interconversion is to exploit Laue crystallography in order to obtain “snapshots” and “movies” of ccNiR and HAO in action. Such an ambitious goal first requires the availability of very large quantities of the enzymes in question. Furthermore, Laue crystallography typically requires crystals of higher quality than those required for conventional crystallography. In particular, low mosaicity is essential in order to interpret the more complex diffraction patterns obtained with polychromatic X-rays. Herein we introduce an expression and purification protocol for obtaining fully active ccNiR from *Shewanella oneidensis* in high yield and purity. We characterize the protein using a variety of techniques, and present the crystal structure obtained using the Laue method.

Materials and Methods

Overexpression of S. oneidensis ccNiR

A DNA sequence encoding for ccNiR was synthesized (Genscript) using codon optimization parameters derived from *E. coli*. The wild-type N-terminal signal peptide was replaced with the signal peptide from the *S. oneidensis* protein “Small Tetra-heme *c*” (STC), which is constitutively expressed in high levels [37, 38]. PCR was performed using Phusion® Hot-Start High-Fidelity DNA polymerase (Finnzymes) and the primers ccNiRopt-F (5’-GACTGAATTCGGAGGATACAATTA-3’) and ccNiRopt-R (5’-GATCTCTAGATCACTTGTAGGTCG-3’). The resulting DNA fragment as well as the plasmid pHSG298 (Takara Bio) were digested with EcoRI and XbaI (New England Biolabs) and ligated together using T4 DNA Ligase (New England Biolabs). The plasmid construct was used to transform chemically-competent NEB5-α cells (New England Biolabs). Positive transformants were selected for by plating onto LB agar plates containing 50μg/mL kanamycin and screened using colony-PCR. Plasmid DNA was isolated from the *E. coli* cells and used to transform electro-competent *S. oneidensis* TSP-C cells (rifampicin-resistant) [39] via electroporation with the Gene-Pulser MXcell Electroporation System® (Bio-Rad). Positive transformants were screened for by plating onto LB agar plates containing 50μg/mL kanamycin, 30μg/mL rifampicin, and 20mM $MgSO_4$. A single colony was used to inoculate a 5 mL overnight culture, which was then used to inoculate multiple 1 L cultures that were harvested after ~20 hours of growth. Cell pellets were re-suspended in

50 mM HEPES, pH 7.0, containing 1mM EDTA, 10 μM leupeptin, and 500 μM AEBSF, and then frozen at −80°C until needed.

Purification of S. oneidensis ccNiR from S. oneidensis TSP-C cells

CcNiR-containing cells were lysed via sonication using a Sonic Dismembrator Model 500 (Fisher Scientific), and centrifuged at 48,000 × *g* for 15 minutes. Ammonium sulfate was added to the supernatant to obtain 50% saturation at 0°C [40], and the sample was again centrifuged. The supernatant was applied to a 2.5 cm × 10 cm Octyl Sepharose column equilibrated with 20mM HEPES, 1mM EDTA, 3 M ammonium sulfate, pH 7.0 (Buffer A). The column was first washed with Buffer A, and then with 40% Buffer B (20mM HEPES, 1mM EDTA, pH 7.0). In each case the wash continued until the absorbance at 280 nm (A_{280}) returned to baseline. Finally, ccNiR was eluted with 80% Buffer B. The ccNiR eluent was exchanged into Buffer B using Ultracell® 10K MWCO centrifugal filters (Millipore) via repeated concentration of the sample and dilution into Buffer B. The sample was then applied to a 1.3 cm × 10 cm Q-Sepharose column and the flow-through was collected and exchanged into Buffer C (20mM HEPES, 1mM EDTA, 2M ammonium sulfate, pH 7.0) using centrifugal filters as previously described. The sample, concentrated to a volume of ~5 mL, was applied to a 1 mL RESOURCE Isopropyl column (GE Healthcare), and a gradient of 0–40% Buffer B was run. CcNiR typically eluted at 20–30% Buffer B, exhibited an A_{410}/A_{280} ratio of >3.8, and ran as a single band when analyzed by SDS-PAGE (Fig. 2a).

Steady-state Kinetic Analysis

Steady-state kinetic parameters for the ccNiR-catalyzed reduction of nitrite or hydroxylamine by methyl viologen monocation radical (MV_{red}) were obtained in a manner similar to that reported previously by Atkinson et al [41]. Briefly: MV_{red} was generated via bulk electrolysis of methyl viologen (MV) at a potential of −550mV vs. the standard hydrogen electrode (SHE). An assay solution buffered at pH 7.0 with 50 mM HEPES, and containing a known concentration of ccNiR (typically 100 pM), ~75 μM MV_{red}, 1 mM MV, and varying substrate concentration (2 – 500 μM for nitrite, 0.5 – 250 mM for hydroxylamine), was then prepared in a cuvette thermostated at 25°C. The final reagent added was MV_{red}, and its addition initiated the reaction. The re-oxidation of MV_{red} was monitored by tracking the absorbance decrease at 600 nm in the visible spectrum. Reactions were completed anaerobically in a nitrogen-filled glovebox (O_2 < 2ppm).

Spectropotentiometry of ccNiR

UV/Vis spectropotentiometry experiments were performed using a BASi Epsilon EC potentiostat to set the potential, and a CARY Bio 50 UV/Vis spectrophotometer to obtain the spectra at each applied potential. The complete apparatus was housed in an anaerobic glove box. Controlled potentiometric electrolysis of the solution was performed in an optically transparent thin-layer electrode (OTTLE) cell, which was a modification of a previously reported design [42, 43], and is described in detail elsewhere [44]. A solution of ccNiR and mediators (Table 1) was prepared in a buffer containing 50mM HEPES, 200mM NaCl, pH 7.0. All mediators were used at concentrations of 25μM, except hexaammineruthenium(III) chloride which had a concentration of 100 μM. UV/Vis spectra in the range from 250nm – 800 nm were collected at 10mV intervals between +50mV and −600mV (vs. SHE). An Ag/AgCl electrode (BASi, Model RE-5B) was used as a reference. Cyclic voltammograms of MV were collected before and after collecting the datasets, and the calculated midpoint potentials were used to account for any drift in the reference electrode (the midpoint potential of MV was taken to be −0.449 V vs SHE [45]). Datasets were also collected with identical mediator solutions in the absence of ccNiR, and these were subtracted from the corresponding ccNiR data sets to account for any spectral changes from the mediators during the titration. The corrected datasets were analyzed using the commercially available

software packages Origin V.6.0 (Microcal Software, Inc), and Mathcad 13 (Mathsoft Engineering and Education, Inc).

Voltammetric analysis of ccNiR adsorbed on an electrode

Protein film voltammetry (PFV) experiments were performed by immobilizing ccNiR on a pyrolytic graphite edge (PGE) electrode. Prior to generation of a protein film, PGE electrodes were polished with an aqueous slurry of 1 μm alumina followed by a brief sonication. Films were generated by pipetting 3 μL concentrated ccNiR onto the electrode, waiting approximately 20 seconds, then pipetting off excess protein solution. The electrode was then immersed in a mixed buffer system (5 mM sodium acetate, MES, MOPS, TAPS, CHES, CAPS; 100 mM NaCl) in a three-electrode water jacketed electrochemical cell. A platinum wire counter-electrode and a saturated calomel reference electrode were used. PFV experiments were performed using a PGSTAT 30 AutoLab (Ecochemie) potentiostat equipped with FRA and ECD modules. PFV experiments were performed on the bench top with argon gas bubbling through the cell solution to remove oxygen. The electrochemical cell was housed in a Faraday cage to reduce noise. Data was collected using the GPES software package (Ecochemie). Cyclic voltammograms produced by PFV experiments were background subtracted to remove electrode capacitance using the SOAS software package [46]. The broad envelope of signal produced by a PFV experiment was deconvoluted by using a fit derived from the Nernst equation, assuming a one-electron contribution of equal surface coverage for each heme of ccNiR.

Crystallization of S. oneidensis MR-1 ccNiR

Initial crystallization screens were performed on ccNiR in the laboratory of Dr. J. Fu (Medical College of Wisconsin) using a robotic high throughput screening system, and the custom in-house screen MCW192. Crystals were obtained from solutions containing 50mM triethanolamine at pH 8.25 with 19% PEG4K. Further optimization of the crystallization conditions was then performed using the hanging drop method, where 2 μL drops were prepared by mixing 1 μL ccNiR stock with 1 μL precipitant solution, and suspended over a reservoir containing 500 μL precipitant. Optimal crystals were obtained when the ccNiR stock had a concentration of 10mg/mL, while the precipitant consisted of a solution containing 50mM triethanolamine and 14% PEG 4K, pH 8.25. Trays of hanging drop samples were incubated at 23° C. Crystals typically appeared overnight. The onset of crystal formation appears to be critically dependent on the temperature; no change in drop appearance was observed at temperatures above 23° C, whereas below this temperature liquid-liquid phase separation invariably occurred. Some batches of purified protein resisted crystallization even at 23° C. In such cases micro-seeding as follows proved useful. Previously grown crystals were pulverized in mother liquor using a 3 mL tissue grinder (Wheaton), and then mixed 1:1 with the ccNiR crystallization solution described above. This solution was incubated at 25° C for 6–18 hours, and then slowly cooled by transferring the sample to a 20° C room. Crystals grown in this manner typically appeared in 2–3 days.

Crystallographic Data Collection

Crystals with dimensions of 200μm × 60μm × 60μm were grown as described above. For conventional crystallographic analysis crystals were cryoprotected by transferring them to a solution of mother liquor supplemented with 10% (w/v) PEG 20K, and then flash frozen. Weak monochromatic crystallographic data to a resolution of 3.2 Å were collected at BioCARS 14BM-C beamline at cryogenic temperatures (100K) using an ADSC Q315 detector. Data were collected in 0.5° steps for a total of 180°. Data were analyzed by Mosflm [47] and scaled and merged by the Collaborative Computational Project Number 4 (CCP4) program 'scala' [48]. Crystals appeared to be monoclinic, spacegroup $P2_1$, with cell

parameters a=47.1 Å b=92.7 Å c=216.5 Å α=90° β=91.04° γ=90°. Data statistics are given in Table 2.

Laue crystallographic data were collected at the BioCARS 14ID-B Laue beamline using X-ray radiation from a double undulator (U23 and U27 [49]). Crystals were mounted in glass capillaries, and data were collected at room temperature. The synchrotron operated in hybrid mode, and radiation from a single electron bunch was selected. Each X-ray pulse contained about 3×10^{10} photons, and 7 pulses were used per Laue diffraction pattern. Waiting time between the pulses was 1 s. After each Laue pattern the crystal was translated along its long axis to expose a fresh volume of crystal to the X-ray beam. The X-ray beam size was 90μm × 60 μm. Laue data extended to a resolution of 2.59 Å with sufficient completeness to 2.72 Å. The complete dataset consisted of 90 Laue patterns covering 180°. Data were indexed, integrated, and scaled by Precognition/Epinorm (RenzResearch). The spacegroup was determined to be $P2_12_12_1$, orthorhombic, with cell parameters a=51.5 Å b=95.5 Å c=223.0 Å α=90° β=90° γ=90°. Data statistics of the Laue data are also given in Table 2.

Results

Overexpression of ccNiR

Several approaches to overexpressing *S. oneidensis* ccNiR were explored in this project. In the ultimately successful approach an optimized ccNiR gene was incorporated into a pHSG298 expression vector, and then *S. oneidensis* (TSP-C strain) was transformed with this vector. PHSG298 is very similar to pUC plasmids, except that the latter use the ampicillin resistance gene as the selective agent for isolating transformed cells, whereas pHSG298 uses the kanamycin resistance gene instead. Attempts to obtain ampicillin-resistant colonies of *S. oneidensis* (containing ccNiR in a pUC18 plasmid) were unsuccessful. The *S. oneidensis* TSP-C strain was used, as it has natural rifampicin resistance and allows for double antibiotic selection of transformed cells.

A comparison between the wild-type and optimized ccNiR genes is provided in Supplementary Material. The most notable difference between the two is that in the optimized gene the ccNiR N-terminal signal sequence for periplasmic translocation has been replaced by the signal sequence for another *S. oneidensis* protein, STC, which is typically expressed in larger amounts than ccNiR [38]. *S. oneidensis* cells transformed with the pHSG298 expression vector containing the optimized gene produced 20–30 fold more ccNiR than untransformed cells. Typical yields were ~20 mg crude ccNiR/L culture for the transformed cells, compared with 0.5–1 mg/L for the untransformed cells. Significantly, *S. oneidensis* TSP-C cells transformed with pHSG298 plasmids containing the wild type ccNiR gene, complete with wild-type signal peptide, did not produce ccNiR in concentrations above the background seen from chromosomal expression.

Purification of overexpressed ccniR

CcNiR was obtained in high yield and purity using a 5-step purification procedure. Most impurities were removed after the third step (hydrophobic interaction chromatography [HIC] using octyl sepharose), as shown in Fig. 2a. One of the remaining impurities (~70 kDa) was removed by passing the protein mixture through a Q-sepharose anion exchange column, which doesn't bind CcNiR; this step also removed other minor impurities. A final HIC step using a high-resolution column brought all remaining impurities down to acceptable background concentrations (Fig. 2a). The overall yield for the purification was typically between 30 – 40% (Fig. 2b) of the initial activity. This translates to 7 – 10 mg of pure ccNiR obtained per liter of cell culture, which is ample for protein-intensive experiments such as crystallography or spectropotentiometry.

Stability of the pure ccNiR was assessed using the steady-state assay described in the following section. Micromolar solutions of the protein are stable for over two weeks at pH 7 and 4° C. Very dilute (nanomolar) solutions kept in microcentrifuge tubes appeared to lose activity with half-lives of about 1.5 h. This apparent loss may be due to slight adsorption of the protein into the matrix of the microcentrifuge tube. Alternatively ccNiR in dilute solutions may slowly dissociate from an active dimeric to an inactive monomeric form. The stability of pure ccNiR did not depend on the presence of added Ca^{2+}.

Steady-state Kinetic Analysis of ccNiR

The steady-state kinetics for ccNiR-catalyzed nitrite and hydroxylamine reduction by MV_{red} were obtained for the purified protein. As expected initial rates showed first-order dependence on [ccNiR], zero-order dependence on [MV_{red}] and hyperbolic dependence on [NO_2^-] and [NH_2OH]. The K_m and k_{cat} values obtained from Michaelis-Menten plots of V_o vs. [NO_2^-] were 23±4 μM and 824±33 s^{-1}, respectively, where the k_{cat} value reflects the number of μmol of NO_2^- turned over per second. For the V_o vs. [NH_2OH] plots the corresponding K_m and k_{cat} values were 8.3±2.4 mM and 2380±160 s^{-1}, respectively. All of these values are similar to the Michaelis-Menten parameters obtained for ccNiR from *E. coli* (K_m = 28 μM, k_{cat} = 770 s^{-1} for NO_2^- and 30 mM, 2380 s^{-1} for NH_2OH [6]).

Initially MV for use in the steady-state experiments was reduced using dithionite. However sulfite, a product of dithionite oxidation, was recently shown to be a substrate for the *E. coli* ccNiR, getting reduced to sulfide albeit at a very slow rate [15]. To date we haven't conclusively shown that the *S. oneidensis* ccNiR can catalyze the reduction of sulfite by MV_{red}; however, what is evident is that sulfite is a competitive inhibitor of the nitrite reduction by MV_{red}. Thus, in experiments where MV_{red} was generated by reduction with dithionite, the obtained K_m values were consistently higher than those obtained when MV_{red} was generated by bulk electrolysis. By contrast, the k_{cat} values were unaffected by choice of protocol. The K_I value for sulfite inhibition of nitrite reductase activity was subsequently determined to be approximately 600 μM, by monitoring the dependence of the observed K_m on sulfite concentration in independent experiments (data not shown).

Spectropotentiometry of ccNiR

For spectropotentiometric analysis the spectrum collected in the absence of an applied potential (that of the fully oxidized protein) was first subtracted from those collected under applied potentials, in order to generate difference spectra. The absorbance difference data collected between 379 nm and 454 nm, for all potentials between +34 mV and −516 mV vs NHE, were then subjected to a global analysis described in detail in Supplementary Material. Briefly, the data were first subjected to singular value decomposition (SVD) [50, 51], which revealed five components above the noise level. The SVD-processed data were next analyzed using a model in which each SVD component is assumed to correlate with the addition of 1 electron to each ccNiR

$$C_n = \frac{C_T \prod_{1}^{n} E_n}{denom} \quad 5a$$

where

$$denom = 1 + E_1\{1 + E_2[1 + E_3[1 + E_4(1 + E_5)]]\} \quad 5b$$

and

$$E_n = \exp\left[\frac{nF}{RT}(\varepsilon_n^0 - \varepsilon_{app})\right] \quad 5c$$

$$\mathbf{\Delta\varepsilon} = \mathbf{\Delta A} \cdot [\mathbf{C_{red}} \cdot (\mathbf{C_{red}^T} \cdot \mathbf{C_{red}})]^{-1} \cdot \frac{1}{l} \quad 6$$

monomer (Scheme 2, Eqs. 5 and 6). Equation 5 is derived from the Nernst equation in exponential form, and correlates C_n with the applied potential (see Supplementary Material). In Eq. 5 $\varepsilon^o{}_n$ is the midpoint potential associated with 1-electron reduction of the $(n-1)^{th}$ reduced species, ε_{app} is the applied potential, and C_T is the total ccNiR concentration in solution. Equation 6 is a matrix version of Beer's law such that: $\mathbf{C_{red}}$ is a matrix of concentrations in which each column corresponds to a unique reduced species and each row to a specific applied potential; $\mathbf{\Delta\varepsilon}$ is an extinction coefficient difference matrix in which each column corresponds to a unique reduced species and each row to a wavelength; $\mathbf{\Delta A}$ is the SVD-processed absorbance difference matrix in which each column contains a spectrum at a fixed applied potential, and each row shows how absorbance varies with potential at a fixed wavelength; and l is a scalar representing the path length of the OTTLE cell. The data were fitted to Eqs. 5 and 6 using a program created with Mathcad 13. This program first allows the user to manually enter trial values of the five midpoint potentials. For a given set of midpoint potential values the program then uses Eq. 5 to calculate the concentration of each reduced species at a given applied potential, and stores the concentrations in $\mathbf{C_{red}}$ (Eq. 6). Next the program calculates the extinction coefficient spectra $\mathbf{\Delta\varepsilon}$ using Eq. 6 [52]. Finally, the program uses l and the $\mathbf{\Delta\varepsilon}$ and $\mathbf{C_{red}}$ matrices to generate an absorbance matrix $\mathbf{\Delta A_{calc}}$, and the sum of squares for $\mathbf{\Delta A} - \mathbf{\Delta A_{calc}}$ is computed. By varying the trial values of the five ccNiR midpoint potentials, this sum of squares can be minimized.

Figure 3 shows the results of the global analysis. Figure 3a compares the experimental and calculated spectra at selected applied potentials, while Fig. 3b shows the fitted ΔA vs. ε_{app} slice at 426 nm. Figure 4a provides the calculated extinction coefficient difference spectra $\mathbf{\Delta\varepsilon_n}$ (the columns of matrix $\mathbf{\Delta\varepsilon}$) for each of the reduced ccNiR species, while Fig. 4b provides the absolute extinction coefficient spectra for the species, obtained by adding the extinction coefficient spectrum of the fully oxidized ccNiR to each of the extinction coefficient difference spectra. Finally, Fig. 4c shows the calculated concentrations of the reduced species C_n as a function of applied potential. Table 3 lists the five calculated midpoint potentials, comparing them with those obtained by direct voltammetric methods (next section), and with those previously reported for *E. coli* ccNiR. The uncertainties quoted for each of the $\varepsilon^o{}_n$ values represent the changes that could be made to each trial $\varepsilon^o{}_n$ without increasing the sum of squares by 0.001 units or more (~6% of the sum of squares value).

The procedure described above was also used to investigate the spectral region from 500 nm – 650 nm, where the characteristic α, β bands are observed for reduced low-spin hemes. The complete analysis is provided as Supplementary Material.

Voltammetric analysis of ccNiR adsorbed on an electrode

PFV experiments performed on *S. oneidensis* ccNiR films in the absence of substrate produced a broad envelope of reversible signals that span approximately 450 mV (Fig. 5a). These signals correspond to the reduction and subsequent oxidation of the heme cofactors within the enzyme, and scan-rate dependencies of the maximal currents indicate that the redox couples are due to adsorbed species (data not shown). The non-turnover voltammograms for *S. oneidensis* ccNiR reported here are similar to data previously

reported for *E. coli* ccNiR [53]. *E. coli* ccNiR voltammograms also appear as a broad envelope of signal spanning approximately the same region of potential; however *E. coli* ccNiR voltammograms are more featured and the range of potential covered is slightly larger than that of *S. oneidensis ccNiR*. The overall shape of *S. oneidensis* ccNiR voltammograms changes with pH, indicating the presence one or more pH-dependent redox centers. At high pH values the envelope appears as a single peak, while at pH values lower than 7 the envelope appears to be composed of two large overlapping peaks. At pH values less than 6 and at 0°C, the envelope of signal can be better resolved and more than two peaks can be observed. This resulting envelope of signal can be deconvoluted as the sum of five one-electron peaks, each corresponding to one of the five hemes in a ccNiR monomer (Fig. 5b). Voltammograms reported for *E. coli* ccNiR also fit to five one-electron centers [53]. Alternate fitting schemes, such as the combination of three one-electron features and one two-electron couple, could not account for the data shown in Fig. 5.

Crystal Structure Model Building and Refinement

For an initial molecular replacement the monoclinic ($P2_1$) monochromatic data obtained at 100 K were used. The A and B subunits (one dimer) of the *E. coli* ccNiR without water or calcium ions were used as a template (*E. coli* ccNiR PDB-ID: 2RDZ). Molecular replacement was attempted to 3.5 Å using the CCP4 program “phaser” [54]. One solution comprising two dimers was identified. The molecular replacement solution was quickly refined using “refmac5” (CCP4 program collection [48]) by rigid body and by conventional refinement including non-crystallographic symmetry restraints. The R_{cryst} settled to 32.9%. No further refinement was attempted due to the poor data quality. However, one dimer consisting of subunits A and B of this initial model was then used for molecular replacement against the Laue data, collected at room temperature. A single, distinct molecular replacement solution was found in the orthorhombic crystal form. After rigid-body refinement of the individual subunits A and B, the resulting model was inspected at positions where differences in the sequence between *E. coli* and *S. oneidensis* ccNiR occur. Differences were immediately visible in the electron density, and the atomic model was modified according to the correct *S. oneidensis* ccNiR sequence. All model manipulations were done using “coot” [55]. The electron density map around residues 170 and 220 could be easily re-traced. Both regions accommodate loops which are different in *E. coli* and *S. oneidensis* ccNiR. Very large difference electron density within the protein indicated the presence of a strong scatterer. The electron density was modeled by a calcium ion in accordance to similar findings for the *E. coli* and other ccNiRs previously characterized crystallographically. Finally, water molecules were inserted. The final R-factor dropped to 19.7% (see Table 2).

Attempts to solve the ccNiR structure using monochromatic crystallographic data collected at cryogenic temperatures (100 K) were considerably less successful than those using the Laue method on data collected at room temperature. A variety of cryoprotectants were tested, including glycerol, MPD, PEG 400, PEG 8K, PEG 20K, mineral oil, and various mixtures of these. The best results were obtained using 10% PEG 20K as the cyoprotectant; however, even with this protectant very weak monochromatic data were collected (see I/sigI and R_{merge} in Table 2). Multiple attempts to collect better monochromatic data failed. At room temperature the diffraction patterns fade away after a few degrees. When comparing the room temperature Laue data to the cryogenic monochromatic data, differences as large as 6.5 Å in cell parameters can be observed. In addition, freezing increases the mosaicity. It is difficult to estimate the mosaicity from the size of the Laue reflections, since factors such as crystal size and crossfire also contribute. However, the software (Precognition) estimated the mosaicity to be around 0.1°, which usually yields good Laue patterns. Freezing then increases the mosaicity to around 1°.

The ccNIR crystallizes as dimers, which form the building blocks of both the orthorhombic and monoclinic crystals. Two dimers occupy similar places in both space groups; however, numerous contacts are established between subunits of individual dimers, whereas contacts between two distinct dimers are few. In $P2_12_12_1$ individual dimers are related by crystallographic symmetry, whereas in $P2_1$ two dimers reside in the same asymmetric unit. The difference is that in $P2_1$ the second dimer is slightly rotated relative to the corresponding dimer position in the orthorhombic form (Supplementary Material). Hence, freezing generates strain in the crystals that breaks the symmetry and increases the mosaicity, although the molecular packing in both crystals remains almost the same. These factors contribute to disorder in the crystals at cryogenic temperatures, increase (decrease) the temperature factor (the Debye-Waller factor), and hence contribute to the limited resolution and poor monochromatic data quality.

Discussion

Overexpression of ccNiR

Numerous strategies for the overexpression of multi-heme *c*-type cytochromes have been proposed [38, 39, 56, 57]. Initially, *E. coli* would appear to be a good organism to use for overexpressing *c*-heme proteins such as ccNiR, and indeed it has been used with some success [57–60]. A major disadvantage of *E. coli* though, is that it expresses the eight cytochrome *c* maturation (CCM) chaperones (ccmA-H) needed to incorporate *c*-type hemes post-translationally into apoproteins only under anaerobic conditions. Londer et al. overcame this problem by using an *E. coli* strain that contains the requisite chaperones within the pEC86 vector; however, ccNiR requires an *additional* three chaperones (nrfEFG) in order to correctly ligate lysine to the active-site heme, and *E. coli* only expresses these anaerobically [61].

Shewanella oneidensis has also been used to overexpress *c* hemes [38, 39, 62–64], and is in many ways a better host for this purpose. Crucially, unlike *E. coli*, this organism expresses both the ccmA-H and the nrfEFG operons even under aerobic conditions. In a suitably overexpressing system, this makes *S. oneidensis* a potential source of large quantities of *c*-hemes, since bacteria typically grow much more rapidly and to higher density under aerobic conditions.

Takayama and Akutsu recently used *S. oneidensis* to overexpress human cytochrome *c* by first substituting the human N-terminal signal peptide with that of the *S. oneidensis* protein STC [38]. They proposed this strategy as a general one for the heterologous expression of *c*-hemes within *S. oneidensis*. Our results suggest that in some cases it may be beneficial to change the N-terminal signal peptide prior to expression, even when the desired protein is from *S. oneidensis* and already has a signal peptide recognized by the bacterial CCM system. When we initially expressed the wild-type ccNiR gene, with its corresponding wild–type signal peptide, in *S. oneidensis*, the expression was no higher than the background seen from chromosomal expression. When the optimized gene bearing the STC signal peptide was used, expression was 20–30 fold above background. It is possible that the overexpression is due to better codon usage in the optimized gene, but for ccNiR the wild-type gene doesn't really show any obvious poor usage sections (Supplementary Material). Instead, we suspect that the STC signal peptide leads to more efficient post-translational modification of the associated protein than the ccNiR signal peptide. For example, the protein responsible for translocating apoproteins across the periplasmic membrane might have more affinity for the STC signal peptide than for the ccNiR signal peptide. One can even see how such affinity variations might evolve: for proteins that are not needed by the bacteria in large quantities, such as the highly efficient ccNiR enzyme, there may be no

evolutionary pressure to develop a signal peptide with high affinity for the translocation machinery.

The hypothesis that the rate of *c*-heme protein maturation can be increased by judicious choice of signal peptide is worthy of more systematic investigation in the future. Indeed it is possible that some other signal peptide, such as that for the highly expressed *S. oneidensis* protein Periplasmic Fumarate Reductase (SO2727), could in general lead to even higher overexpression than the STC peptide.

Electrochemical analysis of ccNiR

As shown in Figs. 3 and 5, the spectropotentiometric and film voltammetric data sets are very well modeled by Scheme 2, which assumes 5 uncoupled reduction events. Attempts to fit either data set with models that incorporated coupled reductions invariably produced poorer fits. Table 3 summarizes the midpoint potentials of *S. oneidenis* ccNiR obtained by spectropotentiometry and film voltammetry, and compares these values to ones previously reported for ccNiR from *E. coli* [6, 65]. For the *S. oneidensis* protein the midpoint potentials obtained by film voltammetry are consistently more positive than those obtained by spectropotentiometry, by anywhere from 30 to 80 mV. Attempts to fit the spectropotentiometric data set using the midpoint potentials obtained by film voltammetry yielded very poor fits. The voltammetric data were collected at pH 6 whereas the potentiometric data were obtained at pH 7, and this may partially explain the observed differences. However, we note that the various sets of midpoint potentials obtained for *E. coli* show similar inter-set variability (Table 3), even though all of those experiments were carried out at pH 7. Indeed, there is more variation between the midpoint potential values obtained from the three *E. coli* ccNiR datasets, or between the values obtained from the two *S. oneidensis* ccNiR datasets, than there is when comparing the *S. oneidensis* midpoint potentials obtained by film voltammetry with those obtained by MCD spectropotentiometry for the *E. coli* ccNiR. We therefore conclude that the ccNiRs from *S. oneidensis* and *E. coli* probably have very similar heme midpoint potentials at both pH 6 and 7, and that the observed differences are primarily due to experimental biases introduced by the various measuring methods. Given the complexity of the systems being investigated, these differences are comparatively minor.

We have found one surprising difference between the UV/Vis spectral characteristics of the *S. oneidensis* ccNiR and those reported for *E. coli* ccNiR. In the *E. coli* enzyme, reduction of the active site heme was reported to produce a distinct signal at 435.5 nm [65], consistent with its EPR identification as a high-spin species [6]. We see no such distinct signal in the *S. oneidensis* ccNiR UV/Vis as the protein is reduced; the five reduced species all have calculated extinction coefficient spectra with maxima below 430 nm, where low-spin ferrous hemes are expected to absorb (Fig. 4). The spectrum of the final reduced species C_5 does shift to significantly longer wavelength, but remains below 430 nm. Moreover, by analogy with the *E. coli* ccNiR, whose reduction potentials have been assigned to specific hemes primarily on the basis of EPR spectropotentiometry [6], we would expect that the active site heme 1 is the second heme reduced ($\varepsilon^o_2 = -0.140$ V). The extinction coefficient difference spectrum of the second reduced species, C_2, has a maximum at 423 nm (Fig 4). However, we do note what could be an important pattern at 435 nm in the calculated extinction coefficient difference spectra (vertical line in Fig. 4a). Reduction of Ox to C_1 results in a small increase in $\Delta\varepsilon_{435}$, which is followed by a significantly bigger increase as C_1 is reduced to C_2. Further reduction of C_2 first to C_3 and then to C_4 results in virtually no change in $\Delta\varepsilon_{435}$, after which there is another sizeable increase as C_4 is reduced to C_5. This final increase in $\Delta\varepsilon_{435}$ can be explained by the shift in λ_{max} as C_4 is reduced to C_5; however, the increase associated with the reduction of C_1 to C_2 arises from the fact that the

C_2 extinction coefficient difference spectrum is broader that the other spectra, with an unusually long tail stretching to longer wavelength.

All of our observations are more easily explained if we don't try to associate each ccNiR reduction step with reduction of a single individual heme. Instead we propose that, for example, in 2-electron reduced ccNiR (species C_2) the two electrons are delocalized among several of the hemes, and that the same may be true for the other stages of reduction. This would explain why the UV/Vis spectral changes associated with reduction of C_1 to C_2 appear to exhibit features characteristic of both low-spin and high-spin ferrohemes. The interpretation is also consistent with the EPR results reported by Bamford et al [6]. For example, these researchers showed that a signal at g = 10.8 observable in parallel mode decreased rapidly to about 20% of its initial intensity at applied potentials of ~ −0.05 – −0.2 V, but then decreased at a much slower rate thereafter. This signal was assigned to the high-spin ferric active site weakly exchange coupled to the low-spin ferric heme 3. Our interpretation would assign the rapid decrease in the g = 10.8 signal to production of the 2-electron reduced ccNiR (C_2), but would allow a fraction of the C_2 population to retain the original ferric heme 1. In this fraction another heme would be reduced instead. The appearance of such a distribution of reduced hemes within a multi-heme complex has been predicted in a theoretical investigation of HAO redox equilibria [16], and is likely to be a common phenomenon.

Structure of S. oneidensis ccNiR

Structure determination of the *S. oneidensis* ccNIR reveals what to our knowledge may be the first case in which room temperature polychromatic Laue X-ray data turned out to be better than monochromatic data collected at cryogenic temperatures. Without Laue crystallography we would have been limited to relatively low quality data with a resolution limit lower than 3 Å. The biggest challenge in cryo-crystallography is to find a good cryo-protectant. If this is difficult, and the overall crystal quality is poor in the first place, most data sets are of low quality and must be discarded. In addition, very often crystals even from the same batch do not scatter equally well. Room temperature monochromatic data collection with crystals held in capillaries, or freely mounted using a humidifier [66] offer one possible way out. Since crystals are not frozen, there is little strain that might generate disorder and increased mosaicity, and consequently data quality can be exquisite. However, we never succeeded in collecting complete monochromatic room-temperature data on this ccNIR, because after a few exposures the diffraction patterns fade away. Laue crystallography offers an alternative when monochromatic data collection at ambient or cryotemperatures obstinately fails. Laue crystallography tends to minimize damage to the crystal caused by the ionizing X-rays. Several publications report the effect of X-ray dose and dose rate on protein crystals [35, 67, 68]. The dose tolerance depends on the rate at which the X-ray dose is administered. The higher the rate the higher the tolerance[67], up to a certain limit where temperature increase and, presumably, hydrogen formation destroys the crystal rapidly [68]. Single-pulse Laue crystallography exhibits the highest peak dose rates at synchrotrons (in the order of 10^{13} Gy/s, [35]), but there is enough waiting time between the X-ray pulses to allow for the temperature to equilibrate and for potential hydrogen to diffuse out of the crystal. The combination of ultra-short brilliant X-ray pulses with about a second waiting time in between, and the displacement of the crystal along its axis to expose a fresh crystal volume, proved to be very advantageous for a successful collection of high-resolution data on this ccNIR.

Crystal structures of ccNiR were previously reported from 3 different branches of the bacterial phylogenetic tree [3–9]. *Sulfurospirillum deleyianum* and *Wollinella succinogenes* are ε-proteobacteria, *Desulfovibrio desulfuricans* and *D. vulgaris* are δ-proteobacteria, and *E. coli* and *S. oneidensis* are γ-proteobacteria [4, 7]. All structures reported so far, including

the *S. oneidensis* form described herein, appear to be functional dimers, and exhibit highly conserved heme arrangements. Figure 6 shows an overlay of the *S. oneidensis* hemes within one monomer with the corresponding *E. coli* hemes. The arrangements of the histidine imidazole planes are of note because they often permit correlations to be made between a heme protein's structure and its EPR spectroscopic features [6, 69]. The heme 2 imidazole planes are very nearly parallel in all of the ccNiRs reported to date, whereas the heme 4 and 5 imidazole planes are closer to perpendicular. Each of these arrangements gives rise to a distinct type of EPR spectrum. The imidazole arrangement of heme 2 is more variable than the others, being the most parallel in the *S. oneidensis* protein and less so in other ccNiRs. This heme is typically magnetically coupled to the high-spin active site, and thus exhibits an anomalous EPR signature [6].

In addition to sharing a common heme arrangement, all ccNiRs reported to date contain a Ca^{2+} ion that lies close to the active site in a highly conserved region of the protein [4]. Figure 7 shows the environment of the Ca^{2+} in *S. oneidensis* ccNiR. The ion is coordinated in bidentate fashion by Glu 205, and in monodentate fashion by the Tyr 206 and Lys 254 backbone carbonyls, and the Gln 256 side-chain carbonyl. In other ccNiRs two remaining (cis-oriented) coordination sites are occupied by waters; however in the *S. oneidensis* structure we only assigned one water to the Ca^{2+} in subunit B. In subunit A the difference electron density that represents this water is very close to the noise level, and it is difficult to identify even one water there. The carbonyl sidechain of Asp 242 and the hydroxyl of Tyr 235 come near to the open calcium coordination sites, but are not within bonding distance. Instead they interact with the water that is weakly coordinated to the Ca^{2+} (see Fig. 7). The ccNiR calcium ions appear to play a vital role in organizing the active site [4], and at least in the case of the *E. coli* protein, mutations to the Ca^{2+} binding amino acids have been shown to affect the active site heme midpoint potential [70]. In the case of ccNiR from *S. deleyianum*, enzyme activity increased in the presence of added calcium, and decreased when chelators such as EDTA were added to the buffers [71]. However the *S. oneidensis* enzyme showed no activity dependence on added calcium, or on the presence of added EDTA. It is not clear from structural comparisons why the Ca^{2+} should be labile in one case and not the other, as the calcium environment is so similar in both cases. In addition to the binding site conserved within all ccNiRs, the ccNiRs from *D. desulfuricans* and *D. vulgaris* exhibit a second, well-defined Ca^{2+} binding site in the vicinity of hemes 3 and 4 [7, 8]. The *E. coli* enzyme crystal structure exhibits a second Ca^{2+} in the same relative position, but the binding site in this case is not as clearly defined, and it is unclear if the calcium is physiologically relevant [6]. We did not detect a second Ca^{2+} ion in the *S. oneidensis* ccNiR, perhaps simply because Ca^{2+} was not included in the crystallization buffer.

Overall, the *S. oneidensis* ccNiR structure is very similar to that of *E. coli*; the structures are compared in Fig. 8. When corresponding subunits of *E.coli* and *S. oneidensis* ccNIRs are compared, the root mean square deviation between the c_α-atoms is 0.7 Å with a 64% sequence identity [72]. A small rectangle on the lower right hand side of the figure highlights the region where the greatest sequence divergence is found. This region of the protein, which borders heme 2, was long suspected to be the entry point for electrons into ccNiR [4]; more recently a crystal structure of *D. vulgaris* ccNiR bound to its physiological partner has all but confirmed this hypothesis [8]. CcNiRs from the different phylogenetic branches use different physiological electron acceptors, which probably explains why the region around heme 2 generally shows significant inter-species sequence variability. CcNiRs from δ and ε proteobacteria use NrfH, a membrane-bound quinol dehydrogenase as the electron donor, while γ-proteobacteria normally use a soluble electron transport protein known as NrfB to shuttle electrons from the membrane-bound quinol dehydrogenase to ccNiR [4]. *S. oneidensis* and *E. coli* are both γ-*proteobacteria*; however the *S. oneidensis* ccNiR is unusual in that its electron donor is a membrane-bound tetraheme protein called

CymA, rather than the more common NrfB [73]. *Shewanella* species appear to have evolved to use a large number of physiological electron donors interchangeably. Accordingly, CymA appears to be a general-purpose protein that can donate electrons equally well to a variety of proteins, such as ccNiR, and nitrate, fumarate and DMSO reductases among others [73].

Summary

We have designed an expression and purification method for obtaining *S. oneidensis* ccNiR from *S. oneidensis* TSP-C strain, which yields 7 – 10 mg of purified protein per liter of culture, enough to sustain protein-intensive research projects such as X-ray crystallography or spectropotentiometry. The purified ccNiR has nitrite and hydroxylamine reductase activities comparable to those previously reported for *E. coli* ccNiR. Spectropotentiometric titration and film voltammetric data are readily fitted assuming 5 independent 1 – electron reduction processes. Global analysis of the spectropotentiometric data suggest that within each reduced species the electrons are distributed amongst the various hemes, rather than being localized on specific heme centers. The purified ccNiR yielded good quality crystals, which allowed us to solve the structure to 2.59 Å using the Laue diffraction method. The structure is similar to that of *E. coli* ccNiR, except in the region where the enzyme interacts with its physiological electron donor. This is expected as different electron donors are used by the two organisms. Efforts are now under way to improve the resolution of the ccNiR Laue structure, obtain structures of the protein in the presence of nitrite, nitric oxide and hydroxylamine, and to develop a method for photoinitiating ccNiR reduction within the crystals, in order to enable time-resolved crystallographic studies. UV/Vis and EPR-spectropotentiometric titrations at various pHs are also under way.

Supplementary Material

Refer to Web version on PubMed Central for supplementary material.

Acknowledgments

MS and AAP are supported by grants NSF-0843459, NSF-1121770 and UWM RGI 101X157. MS is supported by NSF CAREER grant 0952643. ETJ was supported by an NIH-NIGMS National Research Service Award (NRSA) fellowship (1F31GM099416-01). BS and TG gratefully acknowledge support from UW-Milwaukee's Office of Undergraduate Research. Use of the BioCARS Sector 14 was supported by the National Institutes of Health, National Center for Research Resources, under grant number RR007707. The time-resolved set-up at Sector 14 was funded in part through a collaboration with Philip Anfinrud (NIH/NIDDK). Use of the Advanced Photon Source, an Office of Science User Facility operated for the U.S. Department of Energy (DOE) Office of Science by Argonne National Laboratory, was supported by the U.S. DOE under Contract No. DE-AC02-06CH11357. The authors gratefully acknowledge UWM Profs. Nick Silvaggi, Chuck Wimpee, Graham Moran and Daad Safarini for helpful discussions, Mr. Victor Trussell of Rufus King High School for help in stability studies of ccNiR, Nick Silvaggi for the use of his high performance chromatography apparatus, and the Jianhua Fu research group (Medical College of Wisconsin) for the use of their automated crystallization machine in the preliminary crystallization screens.

Abbreviations used

ccNiR	cytochrome *c* nitrite reductase
HAO	hydroxylamine oxidoreductase
AOB	ammonia oxidizing bacteria
MV	methyl viologen
MV_{red}	methyl viologen monocation radical
SHE	standard hydrogen electrode
CCP4	collaborative computational project, number 4

SVD	singular value decomposition
PFV	protein film voltammetry
PGE	pyrolytic graphite edge
AEBSF	4-(2-Aminoethyl) benzenesulfonyl fluoride hydrochloride
CCM	cytochrome c maturation
STC	small tetraheme c

References

1. Schmidt I, Steenbakkers PJM, op den Camp HJM, Schmidt K, Jetten MSM. J. Bacteriol. 2004; 186:2781–2788. [PubMed: 15090520]
2. Ehrlich, HL. Geomicrobiology. New York, NY: Marcel Dekker, Inc; 2002.
3. Einsle O, Messerschmidt A, Stach P, Bourenkov GP, Bartunik HD, Huber R, Kroneck PMH. Nature. 1999; 400:476–480. [PubMed: 10440380]
4. Einsle O, Stach P, Messerschmidt A, Simon J, Kroger A, Huber R, Kroneck PMH. J. Biol. Chem. 2000; 275:39608–39616. [PubMed: 10984487]
5. Pereira I, LeGall J, Xavier A, Teixeira M. Biochim. Biophys. Acta. 2000; 1481:119–130. [PubMed: 11004582]
6. Bamford VA, Angove HC, Seward HE, Thomson AJ, Cole JA, Butt JN, Hemmings AM, Richardson DJ. Biochemistry. 2002; 41:2921–2931. [PubMed: 11863430]
7. Cunha CA, Macieira S, Dias JM, Almeida G, Goncalves LL, Costa C, Lampreia J, Huber R, Moura JJG, Moura I, Romao MJ. J. Biol. Chem. 2003; 278:17455–17465. [PubMed: 12618432]
8. Rodrigues M, Oliveira T, Pereira I, Archer M. EMBO Journal. 2006; 25:5951–5960. [PubMed: 17139260]
9. Rodrigues ML, Oliveira T, Matias PM, Martins C, Valente FM, Pereira IA, Archer M. Acta Cryst. F. 2006; 62:565–568.
10. Igarashi N, Moriyama H, Fujiwara T, Fukumori Y, Tanaka N. Nat. Struct. Biol. 1997; 4:276–284. [PubMed: 9095195]
11. Einsle O, Messerschmidt A, Huber R, Kroneck PMH, Neese F. J. Am. Chem. Soc. 2002; 124:11737–11745. [PubMed: 12296741]
12. Kostera J, Youngblut MD, Slosarczyk JM, Pacheco AA. J. Biol. Inorg. Chem. 2008; 13:1073–1083. [PubMed: 18553112]
13. Kostera J, McGarry JM, Pacheco AA. Biochemistry. 2010; 49:8546–8553. [PubMed: 20812758]
14. Poock S, Leach E, Moir J, Cole J, Richardson D. J. Biol. Chem. 2002; 277:23664–23669. [PubMed: 11960983]
15. Lukat P, Rudolf M, Stach P, Messerschmidt A, Kroneck P, Simon J, Einsle O. Biochemistry. 2008; 47:2080–2086. [PubMed: 18201106]
16. Kurnikov IV, Ratner MA, Pacheco AA. Biochemistry. 2005; 44:1856–1863. [PubMed: 15697211]
17. Bykov D, Neese F. J. Biol. Inorg. Chem. 2011; 16:417–430. [PubMed: 21125303]
18. Ford PC, Lorkovic IM. Chem. Rev. 2002; 102:993–1017. [PubMed: 11942785]
19. Wolak M, van Eldik R. Coord. Chem. Rev. 2002; 230:263–282.
20. Ravelli RBG, McSweeney SM. Structure. 2000; 8:315–328. [PubMed: 10745008]
21. Pearson AR, Pahl R, Kovaleva EG, Davidson VL, Wilmot CM. J. Synchrotron Rad. 2007; 14:92–98.
22. Beitlich T, Kuhnel K, Schulze-Briese C, Shoeman RL, Schlichting I. J. Synchrotron Rad. 2007; 14:11–23.
23. Moffat K, Szebenyi D, Bilderback D. Science. 1984; 223:1423–1425. [PubMed: 17746054]
24. Srajer V, Teng T, Ursby T, Pradervand C, Ren Z, Adachi S, Schildkamp W, Bourgeois D, Wulff M, Moffat K. Science. 1996; 274:1726–1729. [PubMed: 8939867]

25. Ren Z, Bourgeois D, Helliwell JR, Moffat K, Srajer V, Stoddard BL. J. Synchrotron Rad. 1999; 6:891–917.
26. Schmidt M, Rajagopal S, Ren Z, Moffat K. Biophys. J. 2003; 84:2112–2129. [PubMed: 12609912]
27. Schmidt M, Pahl R, Srajer V, Anderson S, Ren Z, Ihee H, Rajagopal S, Moffat K. Proc. Natl. Acad. Sci. U S A. 2004; 101:4799–4804. [PubMed: 15041745]
28. Rajagopal S, Schmidt M, Anderson S, Moffat K. Acta Cryst. D. 2004; 60:860–871. [PubMed: 15103131]
29. Schmidt, M.; Pahl, R.; Ihee, H.; Srajer, V. Protein-ligand interactions: Methods and Applications. Nienhaus, GU., editor. Totowa, NJ: Humana Press; 2005.
30. Rajagopal S, Anderson S, Srajer V, Schmidt M, Pahl R, Moffat K. Structure. 2005; 13:55–63. [PubMed: 15642261]
31. Ihee H, Rajagopal S, Srajer V, Pahl R, Schmidt M, Schotte F, Anfinrud PA, Wulff M, Moffat K. Proc. Natl. Acad. Sci, USA. 2005; 102:7145–7150. [PubMed: 15870207]
32. Key J, Srajer V, Pahl R, Moffat K. Biochemistry. 2007; 46:4706–4715. [PubMed: 17385895]
33. Schmidt, M. Ultrashort Laser Pulses in Medicine and Biology. Zinth, W.; Braun, M.; Gilch, P., editors. Springer Verlag; 2008.
34. Raicu, V.; Schmidt, M.; Stoneman, M. Jakovlev, V. Non-Linear Phenomena. 2008. p. 1-32.
35. Schmidt M, Šrajer V, Purwar N, Tripathi S. J. Synchrotron Rad. 2012; 19 Available online, Jan 2012.
36. Tripathi S, Srajer V, Purwar N, Henning RW, Schmidt M. Biophys. J. 2012; 102:325–332. [PubMed: 22339869]
37. Tsapin AI, Nealson KH, Meyers T, Cusanovich MA, van Beuumen J, Crosby LD, Feinberg BA, Zhang C. J. Bacteriol. 1996; 178:6386–6388. [PubMed: 8892848]
38. Takayama Y, Akutsu H. Protein Expr. Purif. 2007; 56:80–84. [PubMed: 17689099]
39. Ozawa K, Yasukawa F, Fujiwara Y, Akutsu H. Biosci. Biotechnol. Biochem. 2001; 65:185–189. [PubMed: 11272827]
40. Dawson, RMC.; Elliot, DC.; Jones, KM. London: Oxford University Press; 1969.
41. Atkinson SJ, Mowat CG, Reid GA, Chapman SK. FEBS Lett. 2007; 581:3805–3808. [PubMed: 17659281]
42. Heineman WR, Norris BJ, Goelz JF. Anal. Chem. 1975; 47:79–84. [PubMed: 166574]
43. Pilkington MBG, Coles BA, Compton RG. Anal. Chem. 1989; 61:1787–1789.
44. Bodemer, GJ. Ph. D dissertation. Milwaukee, WI: University of Wisconsin-Milwaukee; 2008.
45. Watanabe T, Honda K. J. Phys. Chem. 1982; 86:2617–2619.
46. Fourmond V, Hoke K, Heering HA, Baffert C, Leroux F, Bertrand P, Leger C. Bioelectrochemistry. 2009; 76:141–147. [PubMed: 19328046]
47. Battye TG, Kontogiannis L, Johnson O, Powell HR, Leslie AGW. Acta Cryst. D. 2011; 67:271–281. [PubMed: 21460445]
48. Collaborative Computational Project Number 4. Acta Cryst. D. 1994; 50:760–763. [PubMed: 15299374]
49. Graber T, Anderson S, Brewer H, Chen YS, Cho HS, Dashdorj N, Henning RW, Kosheleva I, Macha G, Meron M, Pahl R, Ren Z, Ruan S, Schotte F, Rajer VS, Viccaro PJ, Westferro F, Anfinrud P, Moffat K. J. Synchrotron Rad. 2011; 18:658–670.
50. Press, WH.; Teukolsky, SA.; Vetterling, WT.; Flannery, BP. New York, NY: Cambridge University Press; 2007. p. 65-75.
51. Henry, ER.; Hofrichter, J. Meth. Enzymol. Brand, L.; Johnson, ML., editors. San Diego: Academic Press; 1992. p. 129-192.
52. Press, WH.; Teukolsky, SA.; Vetterling, WT.; Flannery, BP. New York, NY: Cambridge University Press; 2007. p. 773-839.
53. Gates AJ, Kemp GL, To CY, Mann J, Marritt SJ, Mayes AG, Richardson DJ, Butt JN. Phys. Chem. Chem. Phys. 2011; 13:7720–7731. [PubMed: 21423952]
54. McCoy AJ, Grosse-Kunstleve RW, Adams PD, Winn MD, Storoni LC, Read RJ. J. Appl. Cryst. 2002; 40:658–674. [PubMed: 19461840]

55. Emsley P, Lohkamp B, Scott WG, Cowtan K. Acta Cryst. 2010; D66:486–501.
56. Thony-Meyer L, Fischer F, Kunzler P, Ritz D, Hennecke H. J. Bacteriol. 1995; 177:4321–4326. [PubMed: 7635817]
57. Londer Y, Giuliani SE, Peppler T, Collart FR. Prot. Expr. Purif. 2008; 62:128–137.
58. Londer YY, Pokkuluri PR, Tiede DM, Schiffer M. Biochim. Biophys. acta. 2002; 1554:202–211. [PubMed: 12160993]
59. Londer YY, Pokkuluri PR, Erickson J, Orshonsky V, Schiffer M. Protein Expr. Purif. 2005; 39:254–260. [PubMed: 15642477]
60. Londer YY, Pokkuluri PR, Orshonsky V, Orshonsky L, Schiffer M. Protein Expr. Purif. 2006; 47:241–248. [PubMed: 16403647]
61. Eaves DJ, Grove J, Staudenmann W, James P, Poole RK, White SA, Griffiths L, Cole JA. Mol. Microbiol. 1998; 28:205–216. [PubMed: 9593308]
62. Ozawa K, Tsapin AI, Nealson KH, Cusanovich MA, Akutsu H. Appl. Environ. Microbiol. 2000; 66:4168–4171. [PubMed: 10966450]
63. Shi L, Lin JT, Markillie LM, Squier TC, Hooker BS. BioTechniques. 2005; 38:297–299. [PubMed: 15727136]
64. Shi L, Chen B, Wang Z, Elias DA, Mayer MU, Gorby YA, Ni S, Lower BH, Kennedy DW, Wunschel DS, Mottaz HM, Marshall MJ, Hill EA, Beliaev AS, Zachara JM, Fredrickson JK, Squier TC. J. Bacteriol. 2006; 188:4705–4714. [PubMed: 16788180]
65. Marritt SJ, Kemp GL, Xiaoe L, Durrant JR, Cheesman MR, Butt JN. J. Am. Chem. Soc. 2008; 130:8588–8589. [PubMed: 18549208]
66. Kiefersauer R, Than ME, Dobbek H, Gremer L, Melero M, Strobl S, Dias JM, Soulimane T, Huber R. J. Appl. Cryst. 2000; 33:1223–1230.
67. Southworth-Davies RJ, Medina MA, Carmichael I, Garman EF. Structure. 2007; 15:1531–1541. [PubMed: 18073104]
68. Rajendran C, Dworkowski FS, Wang M, Schulze-Briese C. J. Synchrotron Rad. 2011; 18:318–328.
69. Walker FA. Coord. Chem. Rev. 1999; 186:471–534.
70. Clarke TA, Kemp GL, Van Wonderen JH, Doyle RAS, Cole JA, Tovell N, Cheesman MR, Butt JN, Richardson DJ, Hemmings AM. Biochemistry. 2008; 47:3789–3799. [PubMed: 18311941]
71. Stach P, Einsle O, Schumacher W, Kurun E, Kroneck PMH. J. Inorg. Biochem. 2000; 79:381–385. [PubMed: 10830892]
72. Holm L, Park J. Bioinformatics. 2000; 16:566–567. [PubMed: 10980157]
73. Gao H, Yang ZK, Barua S, Reed SB, Romine MF, Nealson KH, Fredrickson JK, Tiedje JM, Zhou J. ISME Journal. 2009; 3:966–976. [PubMed: 19387485]

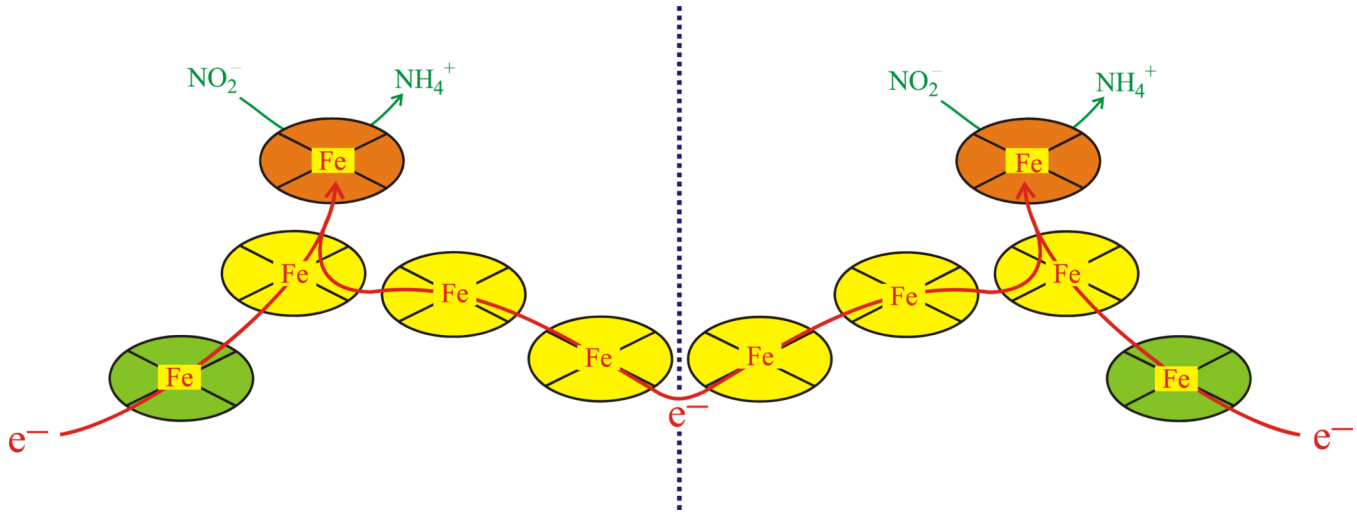

Figure 1.

Arrangement of the 10 hemes within the ccNiR dimer. The yellow and green hemes are 6-coordinate and used for electron transport only, while the two orange hemes are the active sites. The red arrows show likely paths of electron flow. Electrons are believed to enter via the green hemes, but can move between subunits as shown (the dotted line separates the monomeric subunits).

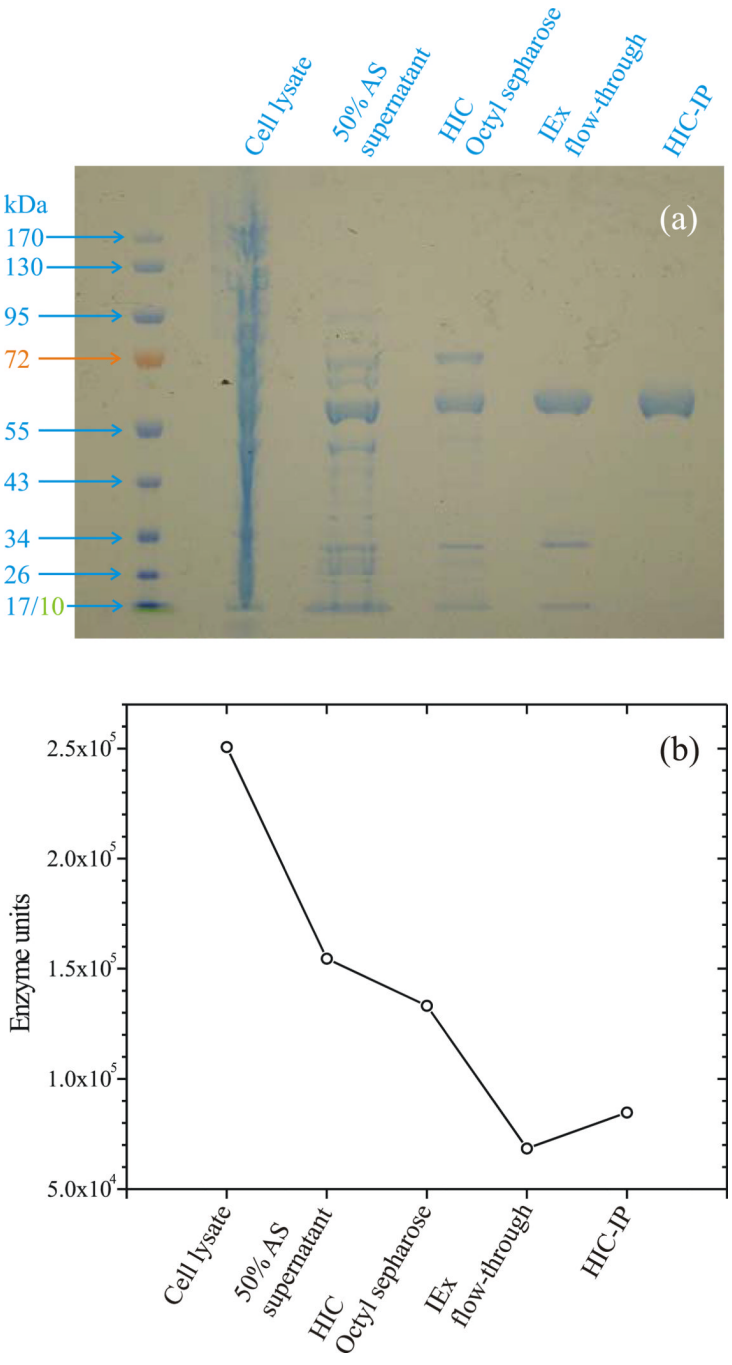

Figure 2.

(a) SDS-Page gel documenting the ccNiR purification procedure; (b) CcNiR activity recovered after each purification step; 1 enzyme unit is the amount required to reduce 1 μmol nitrite per minute under the assay conditons. HIC: hydrophobic interaction chromatography; IEx: ion exchange chromatography; IP: isopropyl.

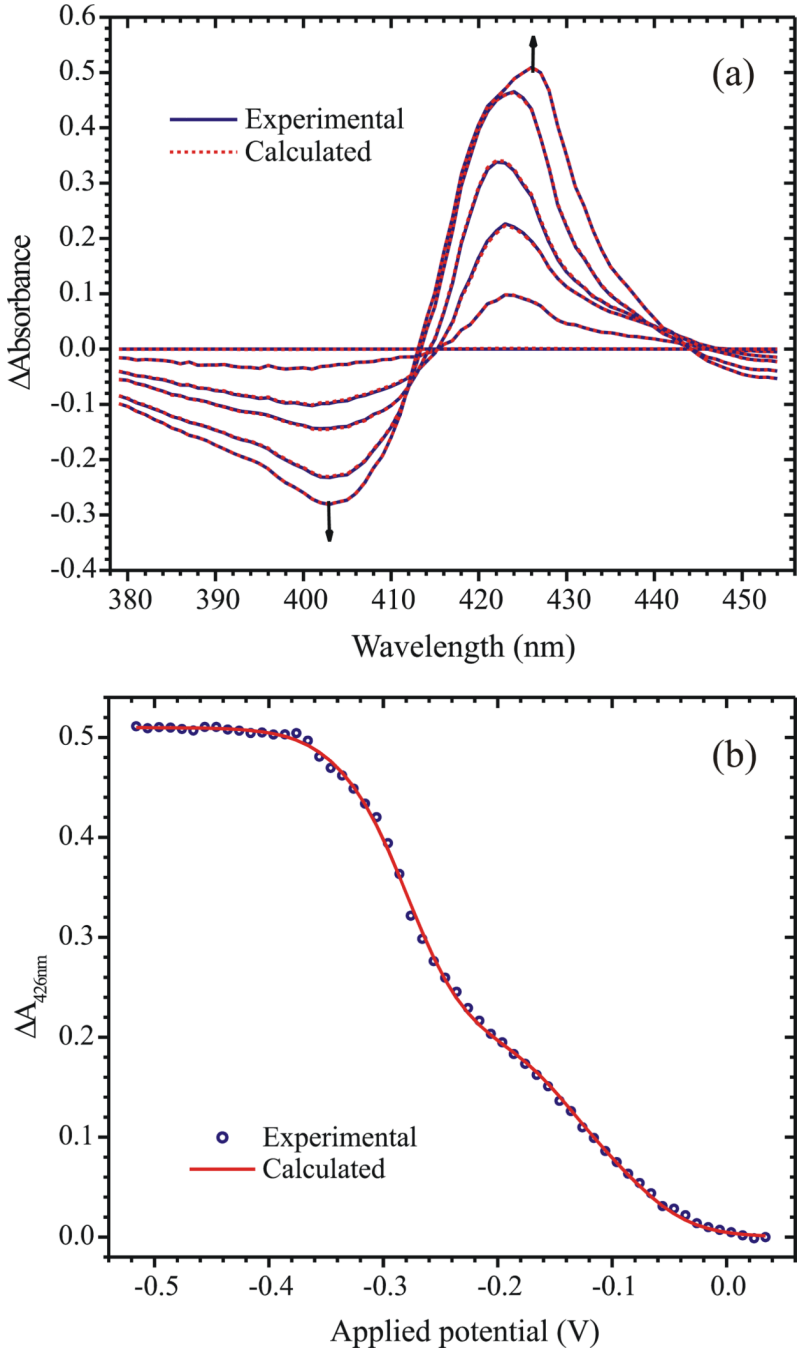

Figure 3.

(a) Spectra obtained at applied potentials of 0.034V, −0.106V, −0.196V, −0.256V, −0.316V and −0.506V vs SHE. Solid blue lines show the experimentally obtained data, while the dashed red lines show the fit obtained using the matrix Eq. 6 (b) The least-squares best fit of the data by Eq. 6 at λ=426 nm.

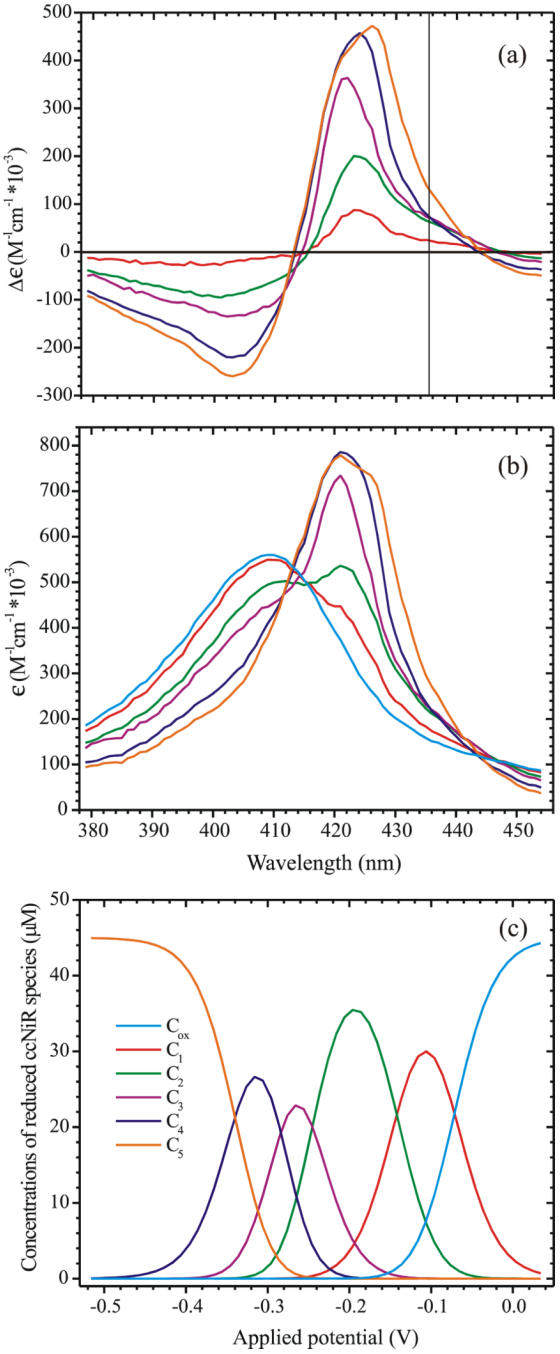

Figure 4.

(a) Extinction coefficient difference spectra corresponding to each of the reduced ccNiR species $C_1 - C_5$ (Scheme 2), as calculated by fitting the experimental spectropotentiometric titration data using Eq. 6. The vertical line shows the point at which a high-spin ferroheme should have an absorbance maximum. (b) Similar to (a), but here the calculated absolute extinction coefficient spectra of $C_1 - C_5$, together with the spectrum of C_{ox}, are shown. (c) Concentrations of the various ccNiR species present in solution at a given applied potential (vs SHE), obtained by fitting the data to Eq. 6.

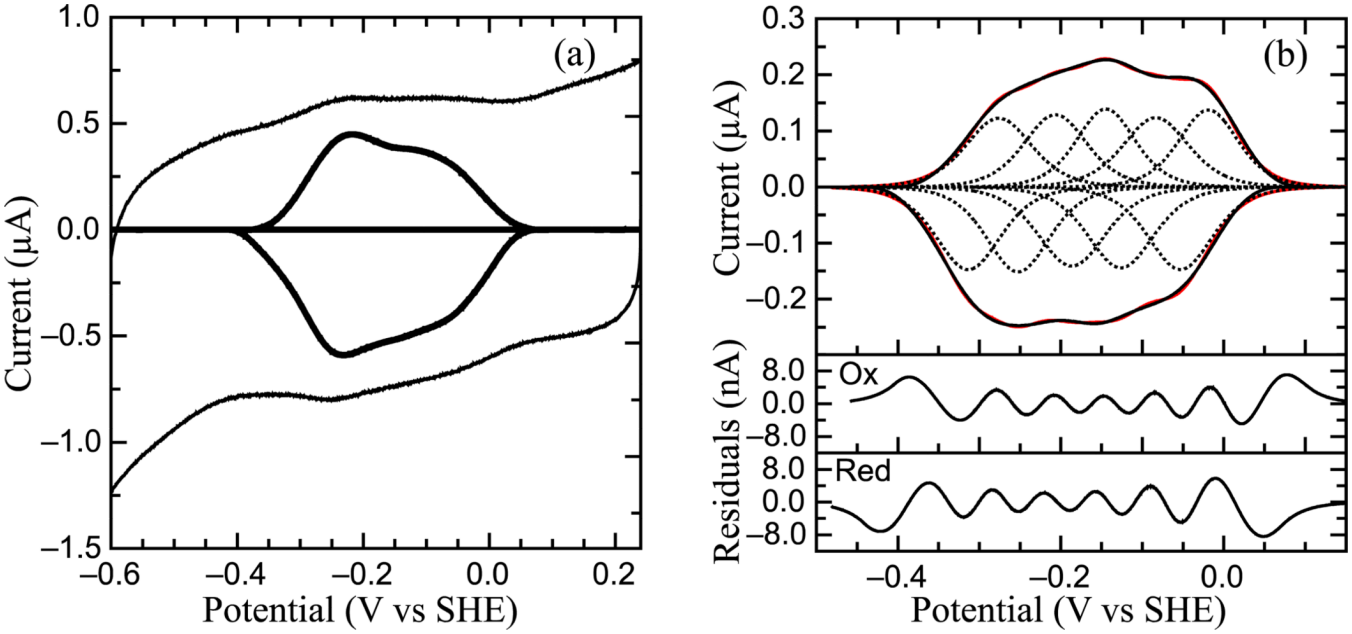

Figure 5.

Protein Film Voltammetry of *S. oneidensis* ccNiR. (a) Typical signal on a graphite electrode. Experiment was carried out at pH 5.15, 0°C, scan rate 45 mV/s. Both the full cyclic voltammogram and background-subtracted data are shown. (b) Baseline-subtracted non-turnover voltammogram recorded at 0°C, pH 6, 250 mV/s. Black trace is the baseline-subtracted voltammogram, red trace and dotted lines are from the resulting fit; equation for fitting derived from the Nernst equation. Sub-plots show the residuals for fits of the oxidative (Ox) and reductive (Red) scans. Calculated E_m values are −0.295 V, −0.230 V, −0.166 V, −0.105 V, and −0.036 V vs. SHE.

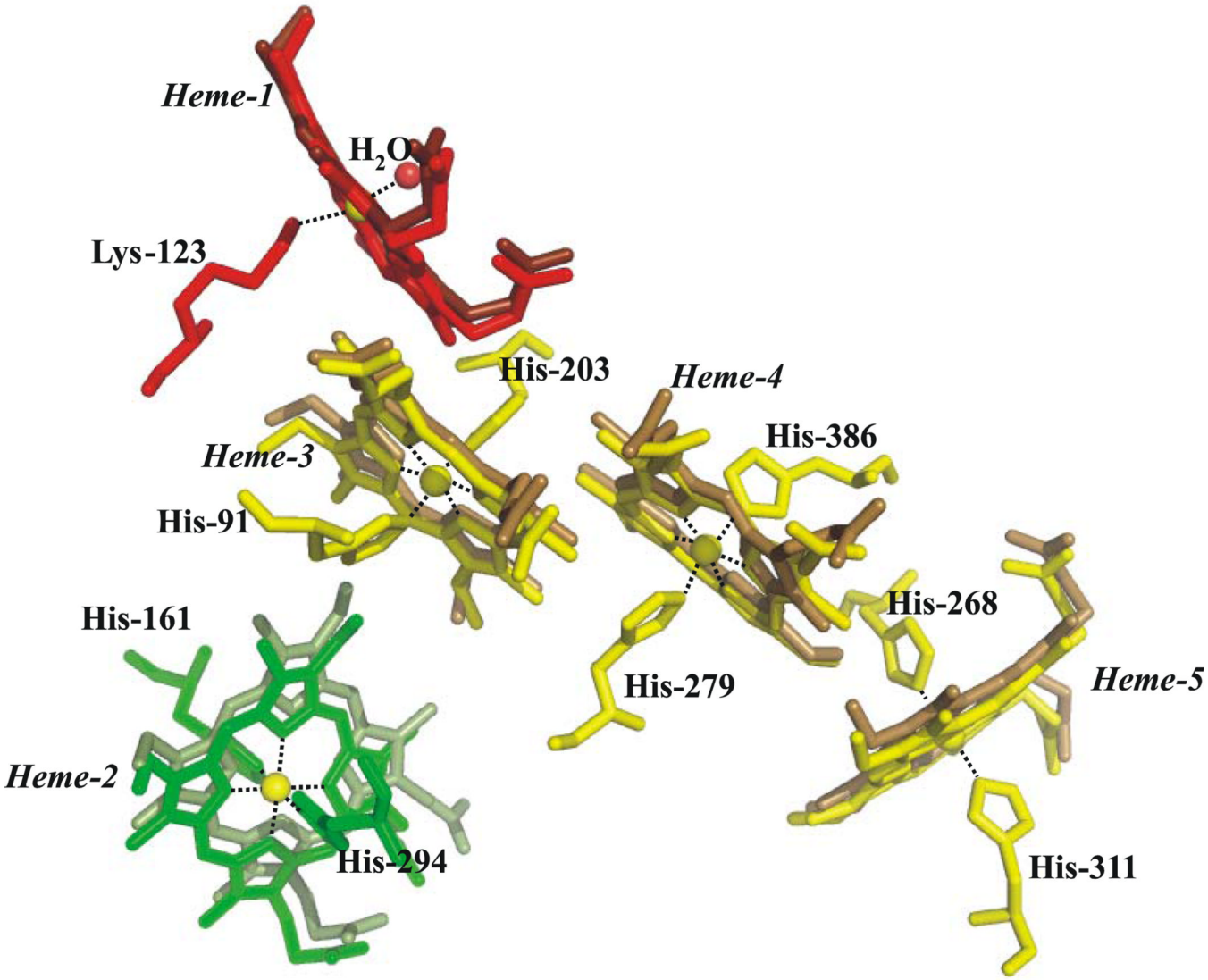

Figure 6.
Comparison between the heme arrangement within a monomer of *S. oneidensis* ccNiR (lighter shade) and that within a monomer of *E. coli* (darker shade). Subunit A is shown. Irons are shown in yellow, while the heme color scheme matches that of Fig. 1.

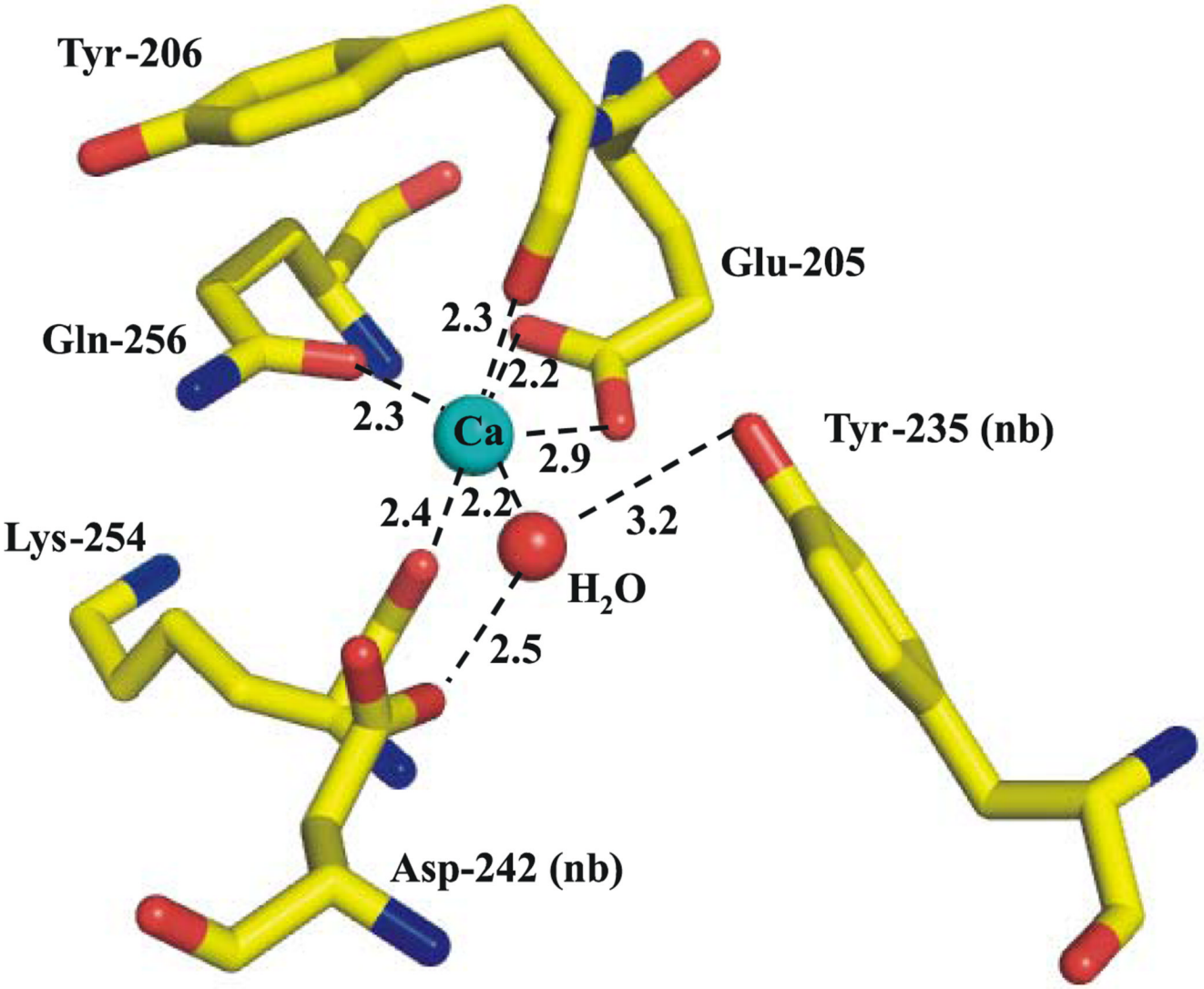

Figure 7.

Coordination environment of the conserved Ca^{2+} site within the *S. oneidensis* ccNiR. Subunit B is shown here; in subunit A the difference electron density feature that corresponds to the Ca-bound water is only 3.5 sigma. This is extremely close to the noise level, and consequently the water was left out of the structure. The *E. coli* structure revealed *two* waters bound to the Ca^{2+}.

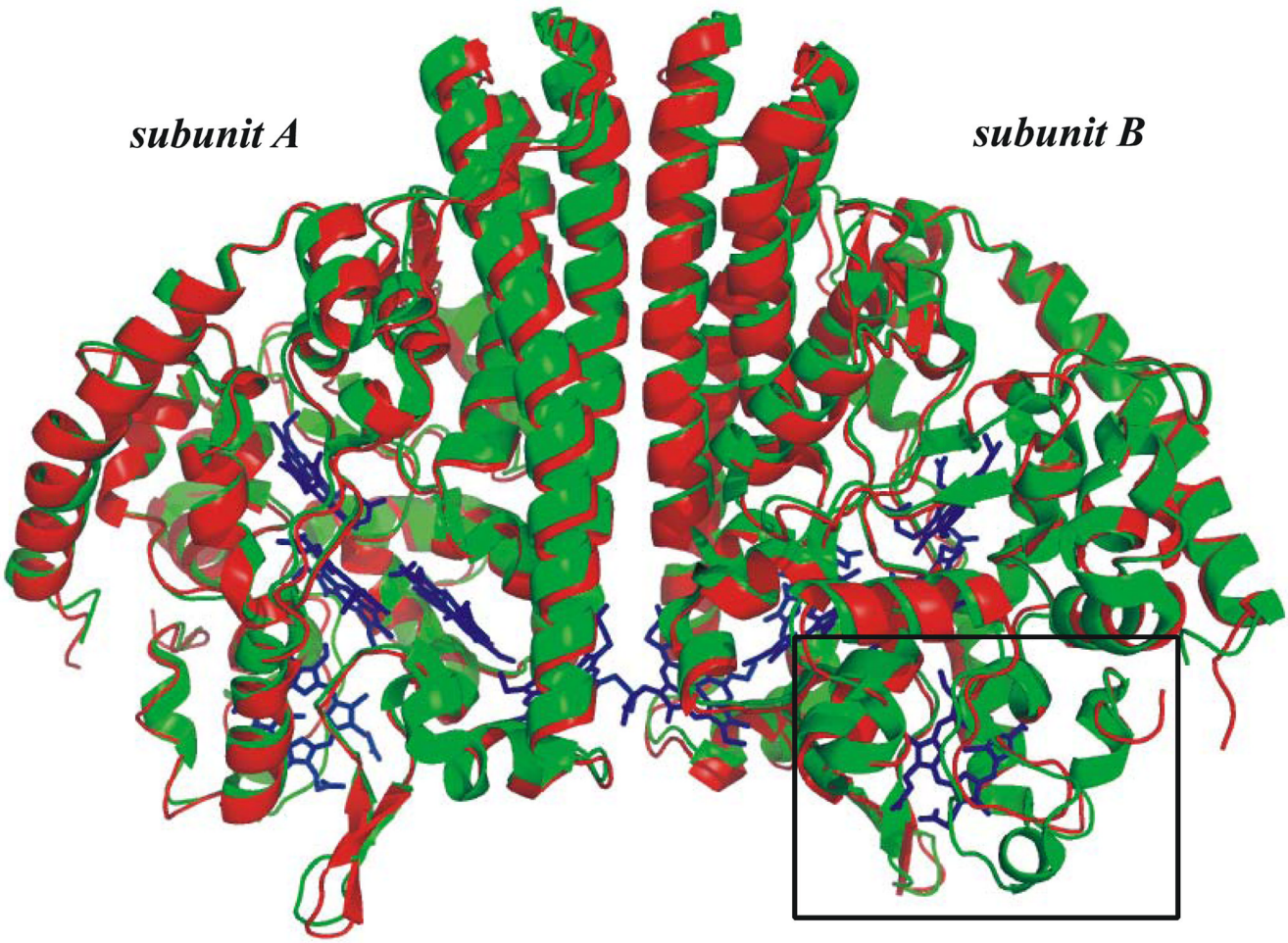

Figure 8.
Overlay comparing the protein structures of *S. oneidensis* and *E. coli* ccNiRs. The rectangle in the lower right-hand side highlights the region near Hemes 2 that shows the greatest sequence divergence.

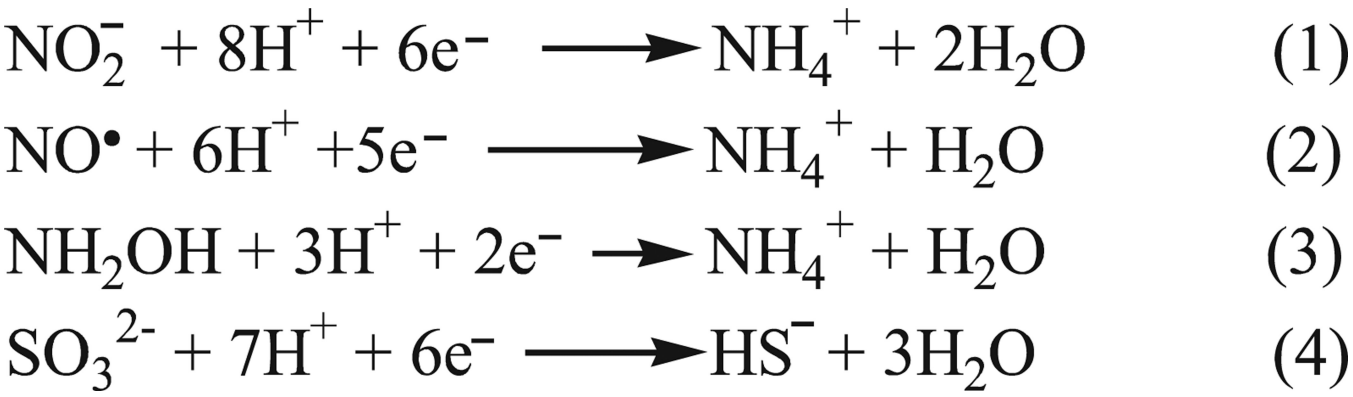

Scheme 1.

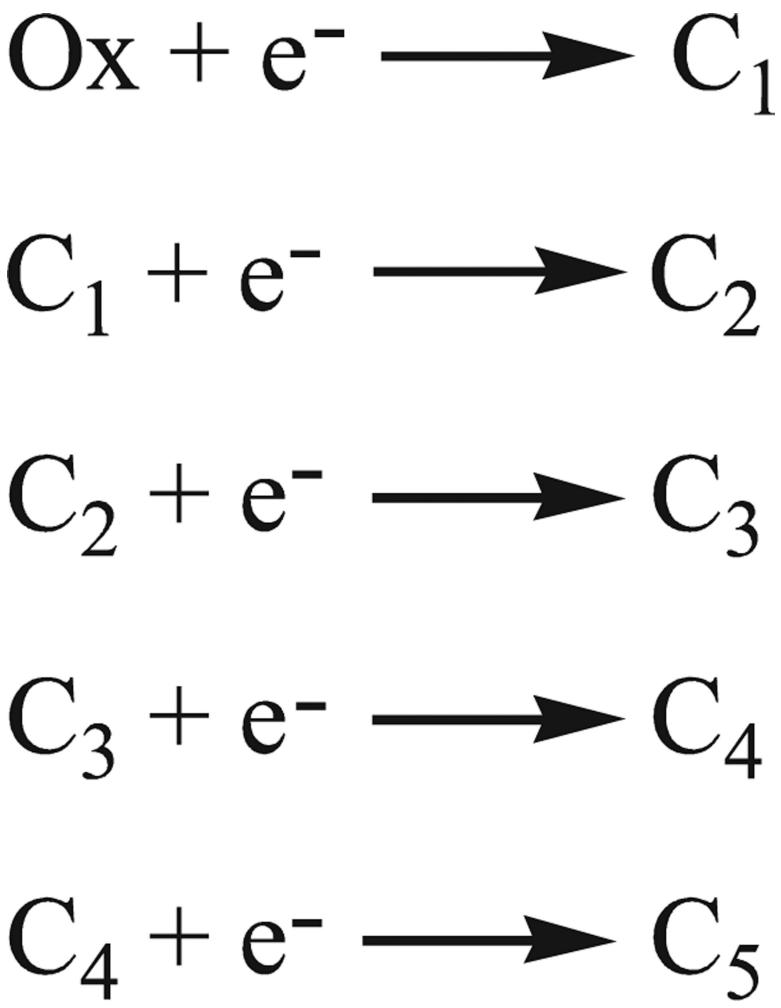

Scheme 2.
Fully oxidized ccNiR is referred to as Ox, while C_1 – C_5 refer to the 1 – 5 electron reduced species, respectively.

Table 1

Mediators used for spectropotentiometry

Mediator	ε^0 (V vs SHE)
Hexaammineruthenium(III) chloride	−0.020
Indigo carmine	−0.125
Anthraquinone 1,5-disulfonic acid	−0.175
Anthraquinone 2-sulfonic acid	−0.255
Safranine O	−0.289
6,7-DPD[1]	−0.390
Methyl viologen	−0.449

1

6,7-DPD: 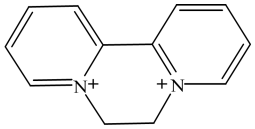

Table 2

Data and refinement statistics

	Monochromatic	**Laue**
Temperature	100 K	273 K
Crystal Size	60 μm × 60 μm × 200 μm	60 μm × 60 μm × 200 μm
Mosaicity [°]	0.9[†]	< 0.1[†]
Resolution	3.20 Å	2.72 Å
cell parameters	a=47.1 Å b=92.7 Å c=216.5 Å α=90° β=91.04° γ=90°	a=51.5 Å b=95.5 Å c=223.0 Å α=90° β=90° γ=90°
V_{cell} [Å^3]	945120	1096769
Space group	$P2_1$ monoclinic	$P2_12_12_1$ orthorhombic
R_{sym}	21.9 %	9.9%
I/sigI	2.3	16.7
Redundancy	2.9	8.9
Completeness (last shell)	73.9 % (63.8 %, 3.37 Å - 3.20 Å)	75.2 % (63.5 %, 2.86 Å – 2.72 Å)
Models for molecular replacement	E. coli ccNIR (2RDZ) subunits A and B	E.coli ccNIR oriented and refined against monochromatic data subunits A and B
asymmetric unit	tetramer	dimer
	R_{cryst}/R-free %	
molecular replacement	47.7 to 3.5 Å	31.1 (to 2.59 Å)[‡]
rigid body	41.1 (to 3.2 Å)	25.6
refinement (no water)	32.9/37.8	21.6/26.7
protein + water		19.7/25.7

[†]As estimated by the data reduction program. Laue: estimated from shape of the reflection, mono + Laue: contain also contributions from beam geometry (crossfire) that might be slightly different at beamlines 14-IDB and 14-BMC.

[‡]Refinement includes all data to 2.59 Å

Table 3

Midpoint potentials of ccNiR hemes (in V vs. SHE) obtained in this work for the *S. oneidensis* protein, and in previous investigations of ccNiR from *E.coli*.

This Work		*E. coli* ccNiR		
Spectropotentiometry	**Film Voltammetry**	**MCD Spectropotentiometry**[1]	**Film Voltammetry**[2]	**EPR Spectropotentiometry**[3]
−0.062±0.007	−0.036	−0.020±0.015 (ls)	+0.022±0.015	−0.037 (ls)
−0.140±0.005	−0.105	−0.108±0.009 (active site)	−0.056±0.015	−0.107 (active site)
−0.25±0.01	−0.166	−0.153±0.011 (ls)	−0.117±0.015	−0.107 (ls)
−0.283±0.007	−0.230	−0.206±0.019 (ls)	−0.189±0.015	−0.323 (ls)
−0.342±0.004	−0.295	−0.292±0.034 (ls)	−0.275±0.015	−0.323 (ls)

[1] Average of two experiments; ref. 65

[2] Ref. 65.

[3] Ref. 6.